Available online at www.sciencedirect.com
SCIENCE DIRECT®
Journal of the Mechanics and Physics of Solids
53 (2005) 2101–2118
JOURNAL OF THE MECHANICS AND PHYSICS OF SOLIDS
www.elsevier.com/locate/jmps

Nonlinear analyses of wrinkles in a film bonded to a compliant substrate

Z.Y. Huang, W. Hong, Z. Suo*

Division of Engineering and Applied Sciences, Harvard University, Cambridge, MA 02138, USA

Received 14 May 2004; accepted 24 March 2005

Abstract

Subject to a compressive membrane force, a film bonded to a compliant substrate often forms a pattern of wrinkles. This paper studies such wrinkles in a layered structure used in several recent experiments. The structure comprises a stiff film bonded to a compliant substrate, which in turn is bonded to a rigid support. Two types of analyses are performed. First, for sinusoidal wrinkles, by minimizing energy, we obtain the wavelength and the amplitude of the wrinkles for substrates of various moduli and thicknesses. Second, we develop a method to simultaneously evolve the two-dimensional pattern in the film and the three-dimensional elastic field in the substrate. The simulations show that the wrinkles can evolve into stripes, labyrinths, or herringbones, depending on the anisotropy of the membrane forces. Statistical averages of the amplitude and wavelength of wrinkles of various patterns correlate well with the analytical solution of the sinusoidal wrinkles.

Keywords: Wrinkles; Thin film; Elastomer; Nonlinear plate; Elasticity

1. Introduction

Consider a film of a stiff material (e.g., a metal) on a substrate of a compliant material (e.g., an elastomer). Subject to a compressive membrane force, the film may

*Corresponding author. Tel.: +1 617 495 3789; fax: +1 617 496 0601.
E-mail address: suo@deas.harvard.edu (Z. Suo).

0022-5096/$ - see front matter © 2005 Elsevier Ltd. All rights reserved.
doi:10.1016/j.jmps.2005.03.007

form a pattern of wrinkles, and remain bonded to the substrate (Bowden et al., 1998). The wrinkles are a nuisance in some applications (Iacopi et al., 2003), but may be used as stretchable interconnects (Watanabe et al., 2002; Lacour et al., 2004), as templates for device fabrication (Yoo et al., 2002; Harrison et al., 2004), or as a means to evaluate mechanical properties of materials (Stafford et al., 2004).

For a film partially debonded from a substrate, when the compressive membrane force exceeds a critical value, the film buckles like an edge-clamped plate; the critical membrane force depends on the size of the debond (Hutchinson and Suo, 1991). As the magnitude of the initial membrane force increases, the debonded film buckles into a complex pattern, and the wavelength decreases (Gioia and Ortiz, 1997; Audoly, 2000). The buckled film may behave like a sheet of crumpled paper (Lobkovsky et al., 1995; Ben Amar and Pomeau, 1997).

By contrast, when a wrinkled film remains bonded to a compliant substrate, the critical membrane force depends on the modulus of the substrate (Allen, 1969). Above the critical condition, as observed experimentally, the bonded film wrinkles into patterns such as stripes, labyrinths and herringbones (Fig. 1), but the wavelength of the individual wrinkles remains practically unchanged as the amplitude of the wrinkles increases (Ohzono and Shimomura, 2004).

This paper focuses on wrinkles in a substrate-bonded film. Specifically, the film is bonded to a compliant substrate, which in turn is bonded to a rigid support (Fig. 2). The substrate thickness, H, can vary by orders of magnitude in applications. The

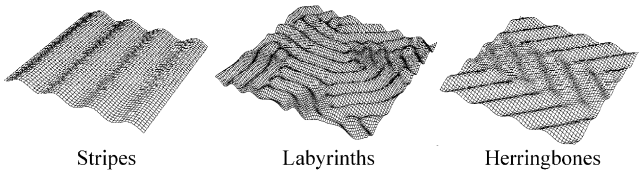

Fig. 1. Schematics of three representative patterns of wrinkles: stripes (a periodic array of straight wrinkles), labyrinths (disordered zigzag wrinkles), and herringbones (a periodic array of zigzag wrinkles).

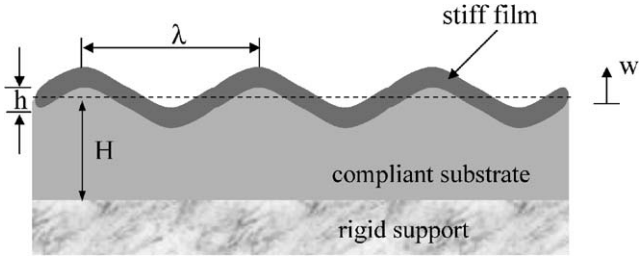

Fig. 2. A stiff film is bonded to a compliant substrate, which in turn is bonded to a rigid support. The film is under in-plane compressive membrane forces. The wrinkle wavelength λ is much larger than the film thickness h. However, the ratio of the wavelength to the substrate thickness, λ/H, can vary from a small fraction to a large number.

layered structure has some practical significance, and has been used in several recent experiments (e.g., Iacopi et al., 2003; Yoo et al., 2002).

Much of the existing theoretical work on substrate-bonded films is based on a linear perturbation analysis, as reviewed by Niu and Talreja (1999). Such an analysis determines the critical membrane force and the wavelength of the wrinkles, but leaves several questions unanswered. What will the amplitude of the wrinkles be? Will the wavelength remain constant as the amplitude increases? What patterns will the wrinkles form?

Several recent nonlinear analyses have attempted to answer these questions. Cerda and Mahadevan (2003), Chen and Hutchinson (2004) and Huang (2005) have calculated the wavelength and amplitude of sinusoidal wrinkles. Using the finite element method, Chen and Hutchinson (2004) have found that the herringbone pattern has the minimum energy among several patterns computed by them. Using numerical simulation and by modeling the substrate as an array of springs and dashpots, Huang et al. (2004) have shown that wrinkles can evolve into several patterns, depending on the anisotropy of the membrane forces.

In this paper, we first calculate the amplitude and wavelength of the sinusoidal wrinkles as functions of the modulus and thickness of the substrate. Our results extend that of Chen and Hutchinson (2004) and Huang (2005) to a film on a substrate of finite thickness, and complement the scaling analysis of Cerda and Mahadevan (2003). We show that the wavelength of the wrinkles remains constant as the amplitude of the wrinkles increases. We then develop a spectral method to evolve two-dimensional patterns of wrinkles. Instead of modeling the substrate as an array of springs and dashpots, we now represent the exact three-dimensional elastic field of the substrate in the Fourier space.

2. Governing equations for the film

When flat, the film is subject to a state of biaxial membrane strains, ε_{11}^0 and ε_{22}^0, taken to be uniform in the film. The principal directions of the strain tensor coincide with the coordinates x_1 and x_2, so that $\varepsilon_{12}^0 = 0$. We take this flat state as the reference, and consider deformation from this state. When the film wrinkles, the wavelength is much larger than the film thickness, so that the von Karman elastic nonlinear plate theory adequately models the film (Landau and Lifshitz, 1959). Let the deflection of the film be w, and the in-plane displacements be u_1 and u_2. The membrane strains $\varepsilon_{\alpha\beta}$ have three contributions: the initial strains, the gradients of the in-plane displacements, and the rotation caused by the deflection, namely,

$$\varepsilon_{\alpha\beta} = \varepsilon_{\alpha\beta}^0 + \frac{1}{2}\left(\frac{\partial u_\alpha}{\partial x_\beta} + \frac{\partial u_\beta}{\partial x_\alpha}\right) + \frac{1}{2}\frac{\partial w}{\partial x_\alpha}\frac{\partial w}{\partial x_\beta}. \tag{1}$$

Each Greek subscript takes values 1 and 2.

Hooke's law relates the membrane forces $N_{\alpha\beta}$ to the membrane strains:

$$N_{\alpha\beta} = h\bar{E}[(1-\nu)\varepsilon_{\alpha\beta} + \nu\varepsilon_{\gamma\gamma}\delta_{\alpha\beta}], \tag{2}$$

where E is Young's modulus, v Poisson's ratio, and h the thickness of the film; $\bar{E} = E/(1-v^2)$. The repeated Greek subscript implies summation over 1 and 2; $\delta_{11} = \delta_{22} = 1$ and $\delta_{12} = \delta_{21} = 0$.

The wrinkled film remains bonded to the substrate. On the film/substrate interface, let T_1 and T_2 be the shear stresses and T_3 be the normal stress. Equilibrium requires that

$$\partial N_{\alpha\beta}/\partial x_\beta = T_\alpha \tag{3}$$

and

$$T_3 = -\frac{h^3\bar{E}}{12}\frac{\partial^4 w}{\partial x_\alpha \partial x_\alpha \partial x_\beta \partial x_\beta} + \frac{\partial}{\partial x_\beta}\left(N_{\alpha\beta}\frac{\partial w}{\partial x_\alpha}\right). \tag{4}$$

3. Sinusoidal wrinkles

Chen and Hutchinson (2004) analyzed sinusoidal wrinkles, of the deflection field $w = A\cos(kx_1)$, in a film on a substrate of infinite thickness, where A is the amplitude and k is the wave number; $\lambda = 2\pi/k$ is the wavelength. The aim of this section is to (a) analyze a film on a substrate of finite thickness, and (b) show that the wavelength of the wrinkles remains constant as the amplitude of the wrinkles increases.

To obtain an analytical solution, following Chen and Hutchinson (2004), we set the shear stresses at the film/substrate interface to be zero. This simplification will be justified in Appendix. When the shear stresses at the interface are taken to be zero, the in-plane equilibrium, Eq. (3), requires that the membrane forces N_{11} and N_{22} be uniform in the film. The membrane strains are also uniform in the film, according to Eq. (2). When $w = A\cos(kx_1)$ is substituted into Eq. (1), the uniformity of the strains requires that the in-plane displacement field be

$$u_1 = \tfrac{1}{8}kA^2\sin(2kx_1), \quad u_2 = 0. \tag{5}$$

The membrane strain field is

$$\varepsilon_{11} = \varepsilon_{11}^0 + \tfrac{1}{4}k^2A^2, \quad \varepsilon_{22} = \varepsilon_{22}^0, \quad \varepsilon_{12} = 0. \tag{6}$$

The membrane forces are

$$N_{11} = N_{11}^0 + \tfrac{1}{4}h\bar{E}k^2A^2, \quad N_{22} = N_{22}^0 + \frac{v}{4}h\bar{E}k^2A^2, \quad N_{12} = 0, \tag{7}$$

where $N_{11}^0 = h\bar{E}(\varepsilon_{11}^0 + v\varepsilon_{22}^0)$ and $N_{22}^0 = h\bar{E}(\varepsilon_{22}^0 + v\varepsilon_{11}^0)$ are the initial membrane forces; the x_1-component is compressive, $N_{11}^0 < 0$. The wrinkles change the in-plane quantities by terms quadratic in the amplitude, A. This dependence is expected from the quadratic contribution of the rotation to the membrane strains, and from the symmetry that a change in the sign of the wrinkle amplitude does not change the in-plane quantities.

We next calculate the average elastic energy per unit area in the wrinkled state. The membrane energy in the film is

$$U^{\mathrm{m}} = \frac{1}{2}(N_{11}\varepsilon_{11} + N_{22}\varepsilon_{22}) = U^0 - \frac{1}{4}|N_{11}^0|k^2A^2 + \frac{h\bar{E}}{32}k^4A^4. \tag{8}$$

The energy in the flat film, $U^0 = (h\bar{E}/2)\lfloor(\varepsilon_{11}^0)^2 + 2\nu\varepsilon_{11}^0\varepsilon_{22}^0 + (\varepsilon_{22}^0)^2\rfloor$, is constant and plays no role in energy minimization. In the wrinkled state, the compressive membrane force reduces the energy. However, the wrinkle stretches the film, giving rise to the last term in Eq. (8), which increases the membrane energy. It is this term that stabilizes the wrinkle amplitude. The bending energy in the film is

$$U^{\mathrm{b}} = \frac{k}{2\pi}\int_0^{2\pi/k}\frac{h^3\bar{E}}{24}\left(\frac{\partial^2 w}{\partial x_1^2}\right)^2 \mathrm{d}x_1 = \frac{h^3\bar{E}}{48}k^4A^2. \tag{9}$$

To account for the substrate of finite thickness, and to show that the wavelength of wrinkles remains constant as the amplitude of the wrinkles increases, we need to deviate from the analysis of Chen and Hutchinson (2004) at this point. We model the substrate as a layer of elastic solid, of thickness H, Young's modulus E_{s}, and Poisson's ratio ν_{s}; $\bar{E}_{\mathrm{s}} = E_{\mathrm{s}}/(1-\nu_{\mathrm{s}}^2)$. Consider the boundary value problem of the substrate, subject to $w = A\cos(kx_1)$ and zero shear stress on the top surface, rigidly constrained on the bottom surface (Fig. 2). We solve the boundary value problem of the elastic field in the substrate by the separation of the variables x_1 and x_3, and find that $T_3 = g\bar{E}_{\mathrm{s}}kw$, with

$$g(kH,\nu_{\mathrm{s}}) = \frac{(3-4\nu_{\mathrm{s}})\cosh(2kH) + 5 - 12\nu_{\mathrm{s}} + 8\nu_{\mathrm{s}}^2 + 2(kH)^2}{(6-8\nu_{\mathrm{s}})\sinh(2kH) - 4kH}. \tag{10}$$

Fig. 3 plots g as a function of kH. This is a monotonically decreasing function. The thicker the substrate, the smaller the normal stress needed to deform the top surface by a certain amount. We will comment on the effect of Poisson's ratio ν_{s} later.The energy in the substrate is

$$U^{\mathrm{s}} = \frac{k}{2\pi}\int_0^{2\pi/k}\frac{1}{2}T_3 w\,\mathrm{d}x_1 = \frac{\bar{E}_{\mathrm{s}}}{4}gkA^2. \tag{11}$$

The sum of the above three contributions gives the total energy of the film/substrate system:

$$U(A,k) = U^0 + \frac{1}{4}(h\bar{E}f - |N_{11}^0|)k^2A^2 + \frac{h\bar{E}}{32}k^4A^4, \tag{12}$$

with

$$f = \frac{(kh)^2}{12} + \frac{g\bar{E}_{\mathrm{s}}}{(kh)\bar{E}}. \tag{13}$$

Similar to a debonded film (Audoly, 2000), the energy for the bonded film and substrate is a fourth order polynomial of A. Fig. 4 sketches this energy as a function of the amplitude of the wrinkles. When $|N_{11}^0| < h\bar{E}f$, the energy minimizes at the state

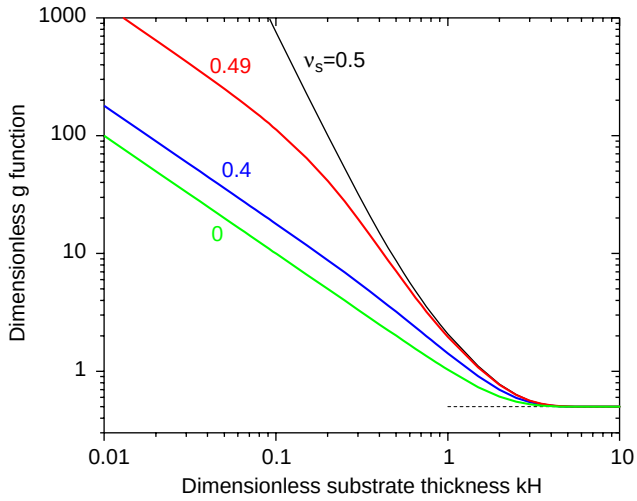

Fig. 3. The dimensionless stiffness g as a function of kH. For a thick substrate, $kH \to \infty$, $g = \frac{1}{2}$. For a thin substrate, $kH \to 0$, $g \sim H^{-1}$ if the substrate, is compressible (e.g., $\nu_s = 0, 0.4, 0.49$), and $g \sim H^{-3}$ if the substrate is incompressible ($\nu_s = 0.5$).

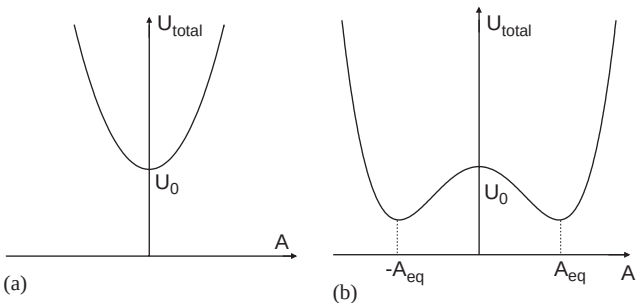

Fig. 4. Sketches of the total energy U as a function of the wrinkle amplitude A. The function has the form $U = U^0 + \alpha(h\bar{E}f - |N_{11}^0|)A^2 + \beta A^4$, where α and β are positive and independent of A. (a) For a small membrane force, $|N_{11}^0| < h\bar{E}f$, the energy minimizes at the state $A = 0$, and the film is flat. (b) For a large membrane force $|N_{11}^0| > h\bar{E}f$, the flat film corresponds to a local energy maximum, and the film wrinkles to an equilibrium amplitude A_{eq}.

$A = 0$, and the film is flat. When $|N_{11}^0| > h\bar{E}f$, the flat film corresponds to a local energy maximum, and the energy minimizes when the film wrinkles with the amplitude

$$A = \frac{2}{k}\sqrt{\frac{|N_{11}^0|}{\bar{E}h} - f}. \tag{14}$$

Inserting (14) into (12), we express the energy as a function of the wave number

$$U(k) = U^0 - \frac{h\bar{E}}{2}\left(\frac{|N_{11}^0|}{h\bar{E}} - f\right)^2. \tag{15}$$

The equilibrium wrinkles select the wave number k_{eq} that minimizes the function $U(k)$ or, equivalently, minimizes the function $f(kh)$. Consequently, the wavelength of the wrinkles in equilibrium is independent of the initial membrane force, and remains constant as the amplitude of the wrinkles increases.

The critical membrane force for the onset of the wrinkles is $N_{\mathrm{c}} \equiv h\bar{E}f_{\min}$, and Eq. (14) becomes

$$A_{\mathrm{eq}} = \frac{2}{k_{\mathrm{eq}}}\sqrt{\frac{|N_{11}^0| - N_{\mathrm{c}}}{\bar{E}h}}. \tag{16}$$

The wrinkle amplitude is quadratic in the excess of the membrane force. Eq. (16) was derived by Chen and Hutchinson (2004) for a film on a substrate of infinite thickness. The above derivation shows that it is also valid for a film on a substrate of finite thickness.

We next describe the results of the analysis, starting with several limiting cases. For a thick substrate, $kH \to \infty$, the wavelength is the only length in the boundary value problem, so that g must be a constant; Eq. (10) gives $g(\nu_{\mathrm{s}}, \infty) = \frac{1}{2}$, which is independent of Poisson's ratio. Minimizing the function f, Eq. (13), we reproduce the thick-substrate limits (Chen and Hutchinson, 2004):

$$\frac{\lambda_{\mathrm{eq}}}{2\pi h} = \left(\frac{\bar{E}}{3\bar{E}_{\mathrm{s}}}\right)^{1/3}, \quad \frac{N_{\mathrm{c}}}{h\bar{E}} = \frac{1}{4}\left(\frac{3\bar{E}_{\mathrm{s}}}{\bar{E}}\right)^{2/3}, \quad \frac{A_{\mathrm{eq}}}{h} = \sqrt{\frac{|N_{11}^0|}{N_{\mathrm{c}}} - 1}. \tag{17}$$

For a thin substrate, $kH \to 0$, the stress field varies slowly in the x_1 direction. This limit can be analyzed using the Winkler model, which represents the substrate as a set of parallel springs, with a stiffness corresponding to that of a layer in a state of uniaxial strain, so that $T_3 = \left[(1-\nu_{\mathrm{s}})^2/(1-2\nu_{\mathrm{s}})\right]\bar{E}_{\mathrm{s}}w/H$. The Winkler model is consistent with Eq. (10), which gives the limit $g(kH, \nu_{\mathrm{s}}) \to \left[(1-\nu_{\mathrm{s}})^2/(1-2\nu_{\mathrm{s}})\right](kH)^{-1}$ as $kH \to 0$. This limit is indicated in Fig. 3 for $\nu_{\mathrm{s}} = 0.0$ and $\nu_{\mathrm{s}} = 0.4$. For this thin-substrate limit, we obtain that

$$\frac{\lambda_{\mathrm{eq}}}{2\pi h} = \left[\frac{H\bar{E}(1-2\nu_{\mathrm{s}})}{12h\bar{E}_{\mathrm{s}}(1-\nu_{\mathrm{s}})^2}\right]^{1/4}, \quad \frac{N_{\mathrm{c}}}{h\bar{E}} = \left[\frac{h\bar{E}_{\mathrm{s}}(1-\nu_{\mathrm{s}})^2}{3H\bar{E}(1-2\nu_{\mathrm{s}})}\right]^{1/2},$$

$$\frac{A_{\mathrm{eq}}}{h} = \sqrt{\frac{2}{3}\left(\frac{|N_{11}^0|}{N_{\mathrm{c}}} - 1\right)}. \tag{18}$$

Poisson's ratio is a dimensionless measure of the degree of compressibility. Compliant materials such as elastomers are nearly incompressible, with $\nu_{\mathrm{s}} \to 0.5$. When the substrate is incompressible, the material is rigid under the uniaxial strain conditions, so that the Winkler model breaks down. Under the sinusoidal stress on the top surface, the substrate does deform, but in a more complicated way. Eq. (10)

is still applicable when $\nu_s = 0.5$, giving the limit $g(kH, 0.5) \to (3/4)(kH)^{-3}$ as $kH \to 0$. In Fig. 3, the thin-substrate limit for an incompressible substrate is indicated with $\nu_s = 0.5$. At $kH = 0.1$, for example, when Poisson's ratio changes from 0.4 to 0.5, g increases by more than an order of magnitude. For a slightly compressible material, $\nu_s = 0.49$ for example, Fig. 3 shows that the g-coefficient approaches the Winkler limit when the substrate thickness is much smaller than the wavelength, but is well approximated by the incompressible limit when the substrate thickness is modestly small compared to the wavelength. When the substrate is incompressible, for the thin-substrate limit, we obtain that

$$\frac{\lambda_{eq}}{2\pi h} = \sqrt{\frac{\bar{H}}{h}}\left(\frac{\bar{E}}{18\bar{E}_s}\right)^{1/6}, \quad \frac{N_c}{h\bar{E}} = \frac{h}{4\bar{H}}\left(\frac{9\bar{E}_s}{4\bar{E}}\right)^{1/3}, \quad \frac{A_{eq}}{h} = \sqrt{\frac{1}{2}\left(\frac{|N_{11}^0|}{N_c} - 1\right)}. \tag{19}$$

The power-law relations in Eqs. (17)–(19) have been predicted by Cerda and Mahadevan (2003) using a scaling analysis. Our calculation provides the explicit coefficients for the specific layered structure.

Given the sensitive dependence on Poisson's ratio discussed above, we caution against the common practice of taking the elastomer as an incompressible material; an accurate Poisson's ratio should be used if the substrate is thin and nearly incompressible. For the same reason, the two thin-substrate limits, Eqs. (18) and (19), should be used with caution. A more reliable approach is to consult the full results for substrates of arbitrary thicknesses, as presented in the following paragraph. On a positive note, the sensitive dependence on Poisson's ratio for wrinkles in a film on a thin substrate may lead to an experimental method to measure Poisson's ratio. Incidentally, wrinkles in a thin film on a thick substrate have been used to measure Young's modulus of the substrate (Stafford et al., 2004).

Fig. 5 plots the critical membrane force N_c, the wavelength λ_{eq}, and the wrinkle amplitude A_{eq} for a compressible substrate ($\nu_s = 0.4$) and for an incompressible substrate ($\nu_s = 0.5$). When the substrate is thick, and the film is much stiffer than the substrate (e.g., $\bar{E}/\bar{E}_s = 10^5$), wrinkles set in when the membrane strain exceeds about 10^{-4}, the wrinkle wavelength is some hundred times the film thickness, and the wrinkle amplitude is on the order of the film thickness. A thinner substrate appears to be stiffer, resulting in a higher critical membrane force, and smaller wrinkle wavelength and amplitude. When the substrate is both thin and incompressible, it appears even stiffer, giving rise to even higher critical membrane forces and smaller wrinkles. Various power laws for the thin-substrate limits are indicated in Fig. 5.

4. Two-dimensional patterns of wrinkles

Huang et al. (2004) simulated the evolution of two-dimensional wrinkle patterns in a film on a thin substrate, using a model of the Winkler type, which represents the substrate as an array of springs and dashpots. This model is valid when the substrate is thin and compressible. We now study wrinkle patterns in a film on a thick substrate by representing the substrate as a three-dimensional elastic solid.

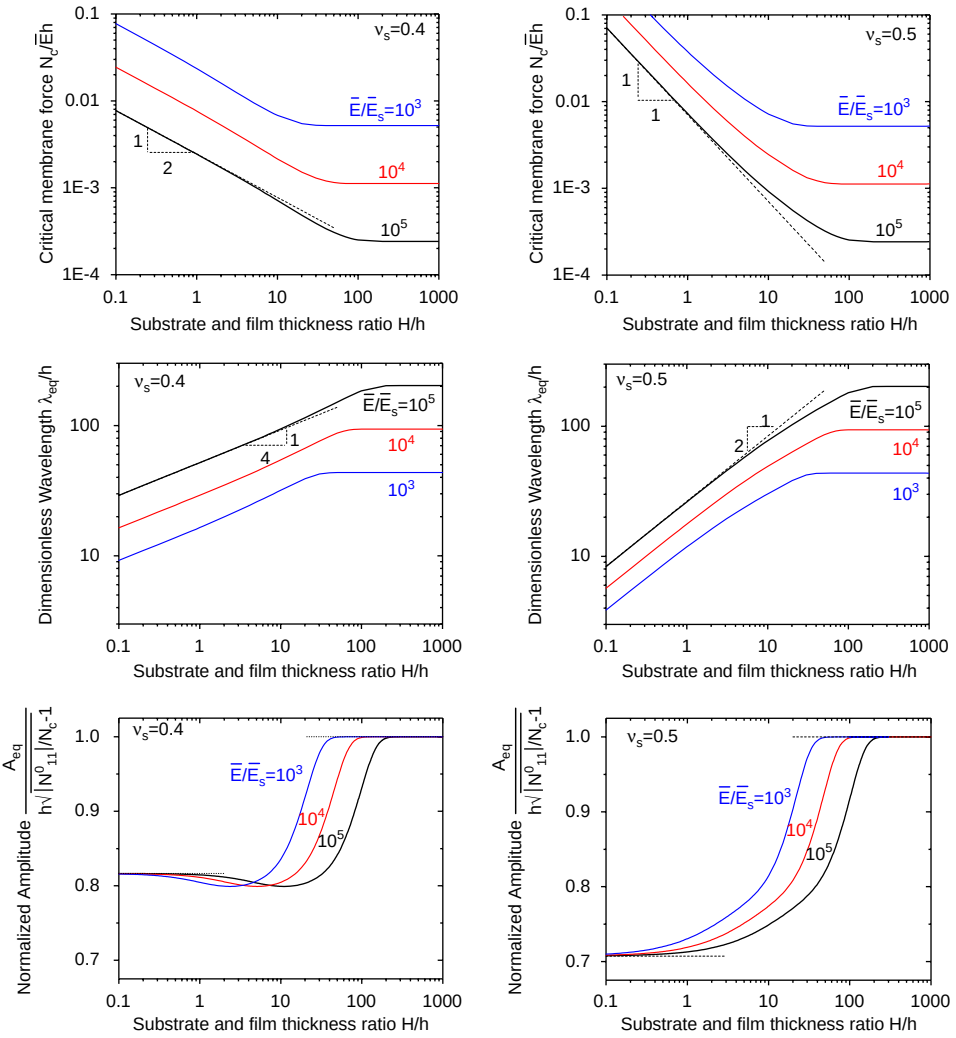

Fig. 5. The critical membrane force, the equilibrium wrinkle wavelength, and the equilibrium wrinkle amplitude are functions of the substrate-to-film thickness ratio. Left column: $\nu_s = 0.4$ (a compressible substrate). Right column: $\nu_s = 0.5$ (an incompressible substrate).

Simulating wrinkle patterns in a film on a thick substrate has three challenges: the nonlinear terms in the plate theory, the high order spatial differentiations in the plate theory, and the three-dimensional elastic field in the substrate. We develop a spectral method that meets these challenges in separate spaces. It calculates the nonlinear terms in the real space. In the Fourier space, the spatial differentiations become multiplications with the wave vector, and the three-dimensional elastic field in the substrate can be solved analytically. The resulting system of equations is nonlinear,

which is solved by using an iterative method. At each iteration, the two spaces communicate via the fast Fourier transform and its inverse.

Define the Fourier transform of a function $w(x_1, x_2)$ as

$$\hat{w}(k_1, k_2) = F[w(x_1, x_2)] = \int_{-\infty}^{\infty}\int_{-\infty}^{\infty} w(x_1, x_2)\exp(-\mathrm{i}k_1x_1 - \mathrm{i}k_2x_2)\,\mathrm{d}x_1\,\mathrm{d}x_2. \tag{20}$$

On the surface of the substrate is prescribed a Fourier component of the displacement vector, $\hat{u}_j\exp(\mathrm{i}k_1x_1 + \mathrm{i}k_2x_2)$, where $\hat{u}_1$ and $\hat{u}_2$ are the amplitudes of the two in-plane displacements, and $\hat{u}_3 \equiv \hat{w}$ is the amplitude of the deflection. In terms of the Fourier component, the elastic field in the substrate can be solved analytically. The Fourier component of the stresses on the surface is give by

$$\hat{T}_i = D_{ij}\hat{u}_j, \tag{21}$$

where

$$D = \frac{\bar{E}_s(1-\nu_s)}{6-8\nu_s}\begin{bmatrix} [4k^2(1-\nu_s)-k_2^2]/k & k_1k_2/k & 2\mathrm{i}k_1(1-2\nu_s) \\ k_1k_2/k & [4k^2(1-\nu_s)-k_1^2]/k & 2\mathrm{i}k_2(1-2\nu_s) \\ -2\mathrm{i}k_1(1-2\nu_s) & -2\mathrm{i}k_2(1-2\nu_s) & 4k(1-\nu_s) \end{bmatrix}, \tag{22}$$

with $k = \sqrt{k_1^2 + k_2^2}$.

In the Fourier space, Eqs. (1)–(3) reduce to a pair of linear algebraic equations for $\hat{u}_1$ and $\hat{u}_2$:

$$C_{\alpha\beta}\hat{u}_\beta = \hat{b}_\alpha \tag{23}$$

with the stiffness matrix

$$C_{\alpha\beta} = 2D_{\alpha\beta} + \bar{E}h\lfloor(1-\nu)k^2\delta_{\alpha\beta} + (1+\nu)k_\alpha k_\beta\rfloor \tag{24}$$

and the force vector

$$b_\alpha = \bar{E}h^3[(1+\nu)w_{,\alpha\gamma}w_{,\gamma} + (1-\nu)w_{,\alpha}w_{,\gamma\gamma} + 2(1-\nu)\varepsilon^0_{\alpha\gamma,\gamma} + 2\nu\varepsilon^0_{\gamma\gamma,\alpha}] - 2D_{\alpha3}w. \tag{25}$$

We will allow the initial membrane strains $\varepsilon^0_{\alpha\beta}$ to be nonuniform.

In the Fourier space, Eq. (4) becomes

$$\left(D_{33} + \frac{\bar{E}h^3k^4}{12}\right)\hat{w} = \mathrm{i}k_\beta F[N_{\alpha\beta}w_{,\alpha}] - D_{3\alpha}\hat{u}_\alpha. \tag{26}$$

We introduce a numerical viscosity to solve the nonlinear algebraic Eq. (26). Adding a term $\zeta\hat{\omega}$ on both sides of Eq. (26), we update $\hat{w}$ by

$$\hat{w}^{n+1} = \left(D_{33} + \frac{\bar{E}h^3k^4}{12} + \zeta\right)^{-1}\{\mathrm{i}k_\beta F[N^n_{\alpha\beta}w^n_{,\alpha}] - D_{3\alpha}\hat{u}^n_\alpha + \zeta\hat{w}^n\}. \tag{27}$$

This procedure in essence is a fixed-point method in computational mathematics. We then calculate $\hat{u}_1^{n+1}$ and $\hat{u}_2^{n+1}$ from Eqs. (23)–(25). The iteration is stopped when the total energy becomes stationary. We set $\zeta = 0.3E_s/h$ for high strain levels and $\zeta =$

$0.03E_s/h$ for small strain levels. Note that our system is nonlinear and contains many degrees of freedom, with a complex energy landscape. The evolution of the patterns will be affected by the detailed dynamics used in computation. However, our simulations from different initial conditions give similar equilibrium patterns. So far as the equilibrium pattern is concerned, the fixed-point method adopted here appears to be adequate.

We calculate wrinkle patterns in a square cell in the plane (x_1, x_2). Periodic boundary conditions replicate the cell to the entire plane. The cell is subdivided into grids. Values of the functions at the grid points are solved by iteration. The cell must

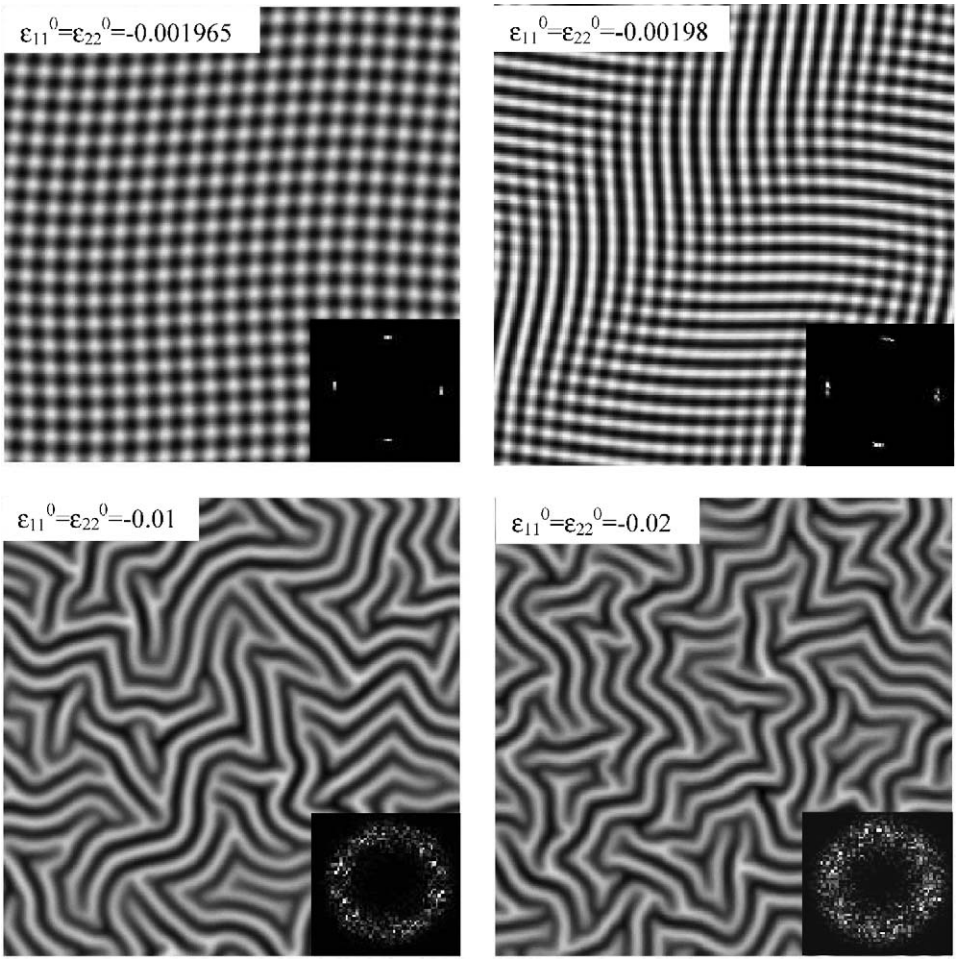

Fig. 6. Wrinkle patterns in films under several levels of isotropic membrane strains. The critical membrane strain is 0.00192. The checkerboard pattern is obtained for the strain magnitude only slight above the critical value. For the labyrinths, the width of each zigzag segment agrees well with the wavelength of the stripe wrinkles, but the length of the segments is several times larger. The insets show the wrinkle amplitude in the Fourier plane.

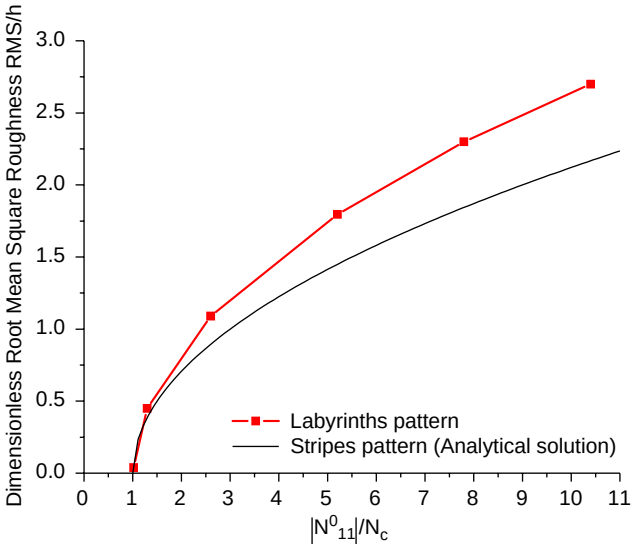

Fig. 7. RMS wrinkle amplitude as a function of the membrane force. For the stripe wrinkles, the numerical simulation agrees well with the analytical solution. For the labyrinth wrinkles, the numerical solution indicates that the RMS wrinkle amplitude is somewhat larger than that of the stripe wrinkles.

be large enough to accommodate many zigzag segments, and the grid spacing must be small enough to resolve the individual elbows. We choose the cell size to be 20 times the equilibrium wavelength, unless stated otherwise. In all computation, $\nu = 0.3$ and $\nu_s = 0.4$.

Fig. 6 shows the wrinkle patterns for films subject to four levels of biaxial membrane strain in the flat state. A gray scale is used: a bright spot represents a crest, and a dark spot a trough. The modulus ratio is $E/E_s = 3250$, giving the critical strain $\varepsilon_c = 0.00192$ and the equilibrium wavelength $\lambda_{eq} = 62.83h$. The calculation cell contains 512 grid points on each side. To initiate the iteration, we prescribe a random deflection field with magnitude below $0.001h$. When the magnitude of the membrane strain is slightly above the critical level, the checkerboard pattern appears. A crest bending equally in all directions, like a spherical cap.

When the magnitude of the membrane strain is large, this symmetry is broken: the crest bends only in one direction, like a cylindrical surface. This symmetry breaking has a geometric origin: a flat sheet can bend to a cylindrical surface with no membrane strain, but can only bend to a spherical surface with severe membrane strains. To relieve compression in all directions, the segments zigzag. As the strain increases, the segment width stays the same, but the segment length decreases.

While the shear stresses at the film/substrate interface have negligible effect on the stripe wrinkles, they play an essential role in stabilizing the two-dimensional wrinkle patterns. Were the shear stresses absent, the compression along the length of a set of segments would be relaxed by the bending of a set of neighboring segments oriented in a different direction. Consequently, the segment length would coarsen indefinitely.

In Fig. 6, the inset in each pattern is a gray scale plot of $\hat{w}^2$ in the Fourier plane (k_1, k_2). A bright spot corresponds to a large value of $\hat{w}^2$. For the checkerboard pattern, the four sharp spots in the Fourier plane correspond to the dominant wavelength in the real-space pattern. For the labyrinth patterns, the circular rings in the Fourier plane correspond to the directional randomness in the real-space patterns, as well as a dominant wavelength. We define the average wavenumber by

$$\bar{k} = \frac{\sum \hat{w}_{\mathrm{mn}}^2 k_{\mathrm{mn}}}{\sum \hat{w}_{\mathrm{mn}}^2}, \tag{28}$$

where k_{mn} is the magnitude of the wave vector at a given grid point, and $\hat{w}_{\mathrm{mn}}$ is the amplitude of the deflection. The summation is over all grid points. For the four

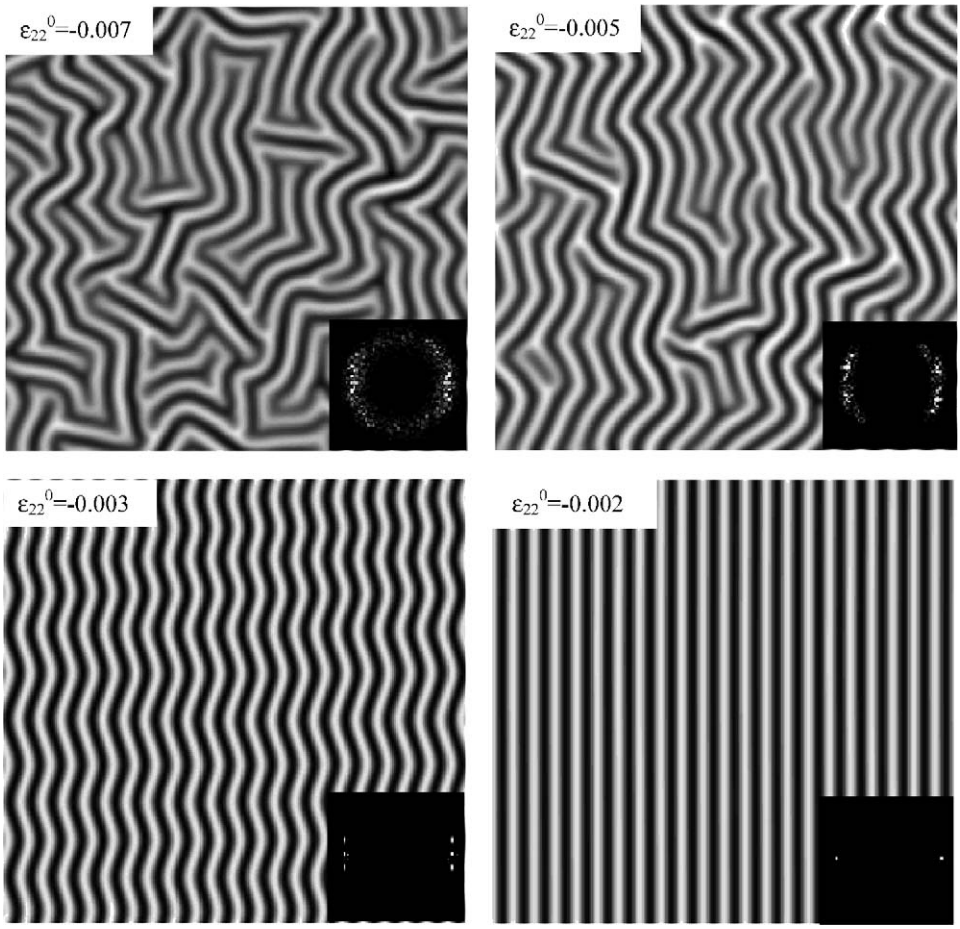

Fig. 8. Wrinkle patterns in films subject to anisotropic membrane strains. In all cases, $\varepsilon_{11}^0 = -0.01$. The directional preference increases as the strains become more anisotropic, from the labyrinths, to the herringbones, and to the stripes. The insets plot the wrinkle amplitude in the Fourier plane.

patterns in Fig. 6, the average wave numbers calculated this way are $1.000k_{eq}$, $1.001k_{eq}$, $1.002k_{eq}$ and $1.002k_{eq}$, respectively. Here k_{eq} is the equilibrium wave number of the stripe wrinkles as calculated in Section 3.

Define the root-mean-square (RMS) deflection by

$$\mathrm{RMS} = \sqrt{\frac{\sum w_{mn}^2}{N}}, \tag{29}$$

where N is the total number of the grid points. The analytical solution of Section 3 gives that $\mathrm{RMS} = h\sqrt{\frac{1}{2}(|N_{11}^0|/N_c - 1)}$ for the sinusoidal stripe wrinkles. Fig. 7 compares the RMS deflection of the labyrinth patterns with that of stripe wrinkles. The data points for the labyrinths are calculated from the patterns shown in Fig. 6. In the numerical simulation of films under isotropic membrane strains, once we prescribe a one-dimensional initial deflection field, the iteration converges to sinusoidal stripes, whose wavelength and amplitude agree well with the analytical solution obtained in Section 3. These comparisons give confidence of the numerical method. More significantly, they show that the analytical solutions in Section 3 can be used to interpret random patterns observe in experiments.

Fig. 8 illustrates the effect of membrane strain state on the wrinkle patterns. In each case, $\varepsilon_{11}^0 = -0.01$, but ε_{22}^0 takes a different value as indicated in the figure. The

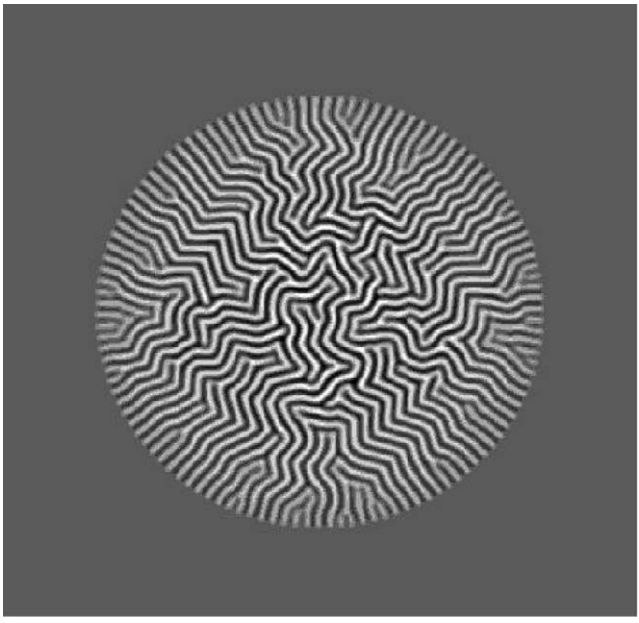

Fig. 9. Wrinkle patterns in a film subject to a nonuniform membrane strain field. The membrane strains are $\varepsilon_{11}^0 = \varepsilon_{22}^0 = -0.02$ inside the circle, and zero outside the circle. The wrinkles arrange into stripes at the perimeter of the circle, herringbones at a distance away from the perimeter, and labyrinths at the center. Very shallow wrinkles form outside the circle.

modulus ratio is $E/E_s = 3250$. At $\varepsilon_{22}^0 = -0.01$, the state of the membrane strain is isotropic, and labyrinths form, similar to patterns shown in Fig. 6. At $\varepsilon_{22}^0 = -0.007$, the symmetry is broken, and wrinkles begin to have some directional preference, which becomes more pronounced at $\varepsilon_{22}^0 = -0.005$. At $\varepsilon_{22}^0 = -0.003$, a perfect array of herringbones forms, with obtuse elbow angles. At $\varepsilon_{22}^0 = -0.002$, stripes form. The gray-scale plots in the Fourier plane show that the directional preference increases as the membrane strain state becomes more anisotropic. Experimentally, the deflection plots in the Fourier plane may be used to evaluate the anisotropy of the membrane strain state.

Fig. 9 illustrates a wrinkle pattern in a film under a nonuniform initial strain field. The simulation conditions mimic those shown experimentally with lithographic patterns (Huck et al., 2000; Chen and Hutchinson, 2004). The radius of circle in Fig. 9 is $19.34\lambda_{eq}$. The computational cell size is $55\lambda_{eq}$. The modulus ratio is $E_1/E_2 = 325$, giving $\lambda_{eq} = 29.16h$ and the critical strain 0.0089. The initial strain in the film is set to be zero outside the circle, and be $\varepsilon_{11}^0 = \varepsilon_{22}^0 = -0.02$ inside the circle. Along the perimeter of the circle, the stress in the radial direction is partially relaxed, so that stripes form. Herringbones form at some distance away from the perimeter. Labyrinths form at the center of the circle.

5. Summary

For sinusoidal wrinkles, the elastic energy of the film-substrate composite is a fourth order polynomial in the wrinkle amplitude, and is a complex function of the wrinkle wavelength. Equilibrium wrinkles select the amplitude and wavelength to minimize the energy. Wrinkles set in when the membrane force reaches a critical value. When the magnitude of the membrane force increases above the critical value, the wrinkle wavelength remains fixed, but the wrinkle amplitude increases with the membrane force. The critical membrane force, the wrinkle wavelength, and wrinkle amplitude are given as function of the elastic constants and substrate thicknesses. We develop a spectral method to simulate two-dimensional wrinkle patterns. When the initial film strains are isotropic, the wrinkles evolve into a pattern with a motif of zigzag segments, in random orientations. When the initial film strains are anisotropic, the wrinkles evolve to an array of herringbones or stripes. The statistical averages of the wrinkle amplitude and wavelength for the random wrinkles correlate well with those given by the analytical solution of the stripe wrinkles.

Acknowledgements

The authors are grateful for the support by the DOE through Grant DE-FG02-03ER46091, by the NSF through the Harvard MRSEC, and by the Division of Engineering and Applied Sciences at Harvard. Discussions with J.W. Hutchinson are valuable.

Appendix

Justification for neglecting the shear stress on the film/substrate interface

In Section 3, to obtain the analytical solution for the sinusoidal wrinkles, we have neglected the shear stress on the film/substrate interface. Here we justify this

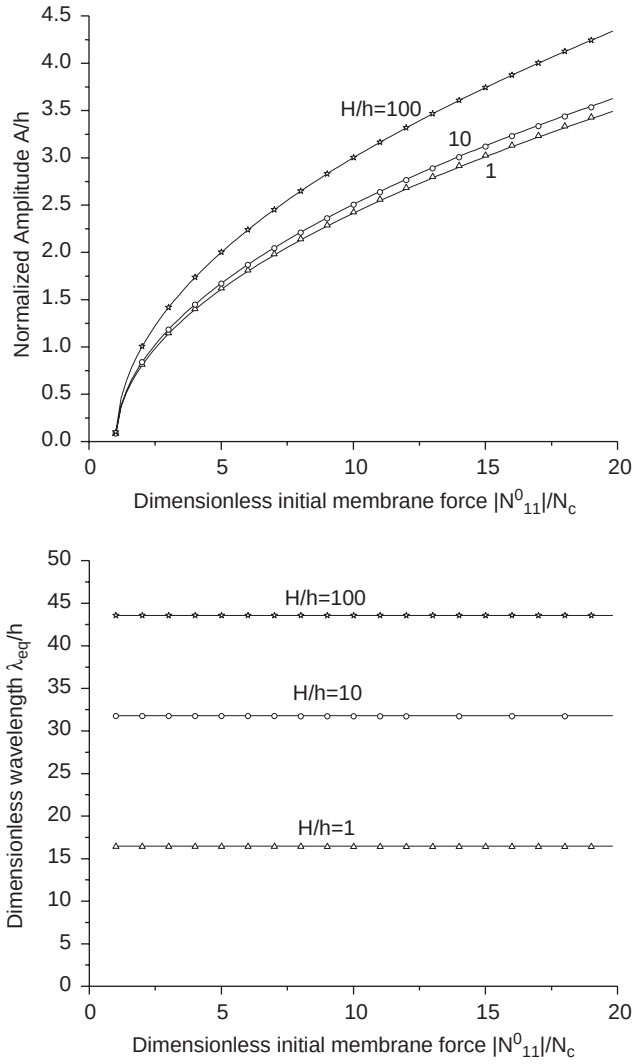

Fig. 10. The amplitude and the wavelength as functions of the initial membrane force. $\bar{E}/\bar{E}_s = 1000$, $v = 0.3, v_s = 0.4$ (compressible substrate). Note that the wavelength remains constant in the postbuckling regime. The solid lines represent the analytical solution, which neglects the shear stress on the film/substrate interface. The various symbols represent the numerical solution, which includes the effect of the shear stress.

simplification by presenting numerical results that allow the shear stress. We represent the displacement field by the Fourier series:

$$u = \sum A_{\mathrm{n}} \cos(nkx_1), \tag{A.1}$$

$$u = \sum B_{\mathrm{n}} \sin(nkx_1). \tag{A.2}$$

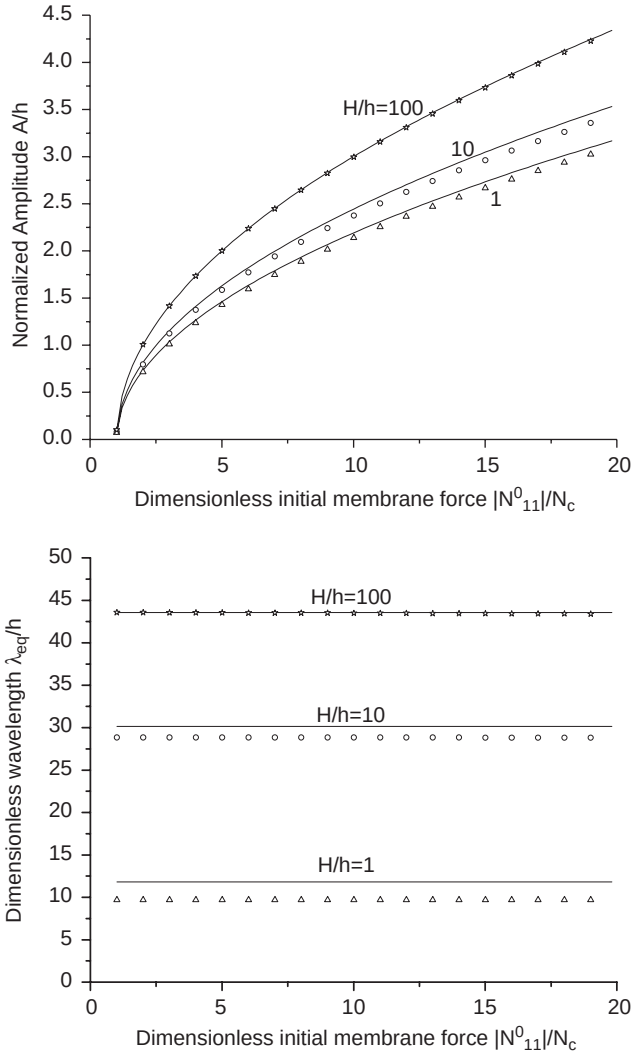

Fig. 11. The amplitude and the wavelength as functions of the initial membrane force. $\bar{E}/\bar{E}_{\mathrm{s}} = 1000$, $v = 0.3, v_{\mathrm{s}} = 0.5$ (incompressible substrate). The solid lines represent the analytical solution. The various symbols represent the numerical solution.

Following the procedure similar to that outlined in Section 3, but including multiple Fourier components and the shear stress, we express the total energy as a function of A_n, B_n and k. These quantities are determined by minimizing the total energy. In numerical calculations, we obtain convergent results by using the first three terms in each of the above Fourier series. Figs. 10 and 11 compare the numerical solution to the analytical solution obtained in Section 3. The agreement is excellent except when the substrate is thin and incompressible. This agreement shows that the analytical solution in Section 3 is a good approximation.

References

Allen, H.G., 1969. Analysis and Design of Structural Sandwich Panels. Pergamon, New York.

Audoly, B., 2000. Mode-dependent toughness and delamination of compressed thin films. J. Mech. Phys. Solids 48, 2315–2332.

Ben Amar, M., Pomeau, Y., 1997. Crumpled paper. Proc. R. Soc. Lond. A 453, 729–755.

Bowden, N., Brittain, S., Evans, A.G., Hutchinson, J.W., Whitesides, G.M., 1998. Spontaneous formation of ordered structures in thin films of metals supported on an elastomeric polymer. Nature 393, 146–149.

Cerda, E., Mahadevan, L., 2003. Geometry and physics of wrinkling. Phys. Rev. Lett. 90, 074302.

Chen, X., Hutchinson, J.W., 2004. Herringbone buckling patterns of compressed thin films on compliant substrates. ASME J. Appl. Mech. 71, 597–603.

Gioia, G., Ortiz, M., 1997. Delamination of compressed thin films. Adv. Appl. Mech. 33, 119–192.

Harrison, C., Stafford, C.M., Zhang, W.H., Karim, A., 2004. Sinusoidal phase grating created by a tunably buckled surface. Appl. Phys. Lett. 85, 4016–4018.

Huang, R., 2005. Kinetic wrinkling of an elastic film on a viscoelastic substrate. J. Mech. Phys. Solids 53, 63–89.

Huang, Z.Y., Hong, W., Suo, Z., 2004. Evolution of wrinkles in hard films on soft substrates. Phys. Rev. E 70, 030601(R).

Huck, W.T.S., Bowden, N., Onck, P., Pardoen, T., Hutchinson, J.W., Whitesides, G.M., 2000. Ordering of spontaneously formed buckles on planar surfaces. Langmuir 16, 3497–3501.

Hutchinson, J.W., Suo, Z., 1991. Mixed-mode cracking in layered materials. Adv. Appl. Mech. 29, 63–191.

Iacopi, F., Brongersma, S.H., Maex, K., 2003. Compressive stress relaxation through buckling of a low-k polymer-thin cap layer system. Appl. Phys. Lett. 82, 1380–1382.

Lacour, S.P., Jones, J., Suo, Z., Wagner, S., 2004. Design and performance of thin metal film interconnects for skin-like electronic circuits. IEEE Electron Device Lett. 25, 179–181.

Landau, L.D., Lifshitz, E.M., 1959. Theory of Elasticity. Pergamon, London.

Lobkovsky, A., Gentges, S., Li, S.H., Morse, D., Witten, T., 1995. Scaling properties of stretching ridges in a crumpled elastic sheet. Science 270, 1482–1484.

Niu, K., Talreja, R.J., 1999. Modeling of wrinkling in sandwich panels under compression. J. Eng. Mech. 125, 875–883.

Ohzono, T., Shimomura, M., 2004. Ordering of microwrinkle patterns by compressive strain. Phys. Rev. B 69, 132202.

Stafford, C.M., Harrison, C., Beers, K.L., Karim, A., Amis, E.J., Vanlandingham, M.R., Kim, H.C., Volksen, W., Miller, R.D., Simonyi, E.E., 2004. A buckling-based metrology for measuring the elastic moduli of polymeric thin films. Nature Mater. 3, 545–550.

Watanabe, M., Shirai, H., Hirai, T., 2002. Wrinkled polypyrrole electrode for electroactive polymer actuators. J. Appl. Phys. 92, 4631–4637.

Yoo, P.J., Suh, K.Y., Park, S.Y., Lee, H.H., 2002. Physical self-assembly of microstructures by anisotropic buckling. Adv. Mater. 14 (19), 1383–1387.